Raman and electronic Raman spectra of lanthanide ions in elpasolite lattices

Peter A. Tanner
Department of Biology and Chemistry, City University of Hong Kong, Tat Chee Avenue, Kowloon, Hong Kong

Xia Shangda
Department of Physics, University of Science and Technology of China, Hefei, Anhui, China

Liu Yu-long
Department of Biology and Chemistry, City University of Hong Kong, Tat Chee Avenue, Kowloon, Hong Kong

Ma Yi
Department of Physics, University of Science and Technology of China, Hefei, Anhui, China

(Received 28 May 1996; revised manuscript received 30 September 1996)

Raman spectra have been recorded from 300–10 K for lanthanide hexachloroelpasolites, Cs_2NaLCl_6. Electronic Raman-scattering intensity ratios have been calculated using Judd-Ofelt-Axe theory and are in reasonable agreement with experimental results, except for those cases where electron-phonon coupling has important consequences. Bands resulting from temperature-dependent electron-phonon coupling phenomena have been observed not only in the Raman spectrum of $Cs_2NaYbCl_6$ but also in that of $Cs_2NaTmCl_6$, and the interaction mechanism is discussed. The coupling element between the coupled $a\Gamma_5 \sim \Gamma_1 + \nu_5$ phonon-electron states of $^3H_6$ in $Cs_2NaTmCl_6$ is estimated to be 20 cm^{-1}, and the corrected wave functions for these coupled states enable a consistent reinterpretation to be made of the optical spectra of $TmCl_6^{3-}$. Excited-state electronic Raman scattering has been observed in the 120-K Raman spectrum of $Cs_2NaTmCl_6$. Using fixed wavelength argon-ion laser lines, there is evidence for a small resonance enhancement of electronic Raman-scattering intensity, and the unusual mechanism for this is discussed. The mixed crystal system $Cs_2NaGd_{1-x}Yb_xCl_6$ exhibits unimodal behavior for the ν_1 and ν_5 vibrations, and the more complex behavior of features in the neighborhood of ν_2 is described. The vibrational energies of the gerade internal LCl_6^{3-} modes (determined from Raman spectra) vary linearly with atomic number of L, except where electron-phonon coupling effects occur. [S0163-1829(97)00218-X]

I. INTRODUCTION

Amberger and co-workers have studied the vibrational and electronic Raman spectra of lanthanide ions, L^{3+}, in crystalline elpasolite lattices,[1,2] providing information useful for studies of the vibrational force-field and the low-lying multiplet term crystal-field parameters. The lanthanide ions are situated at octahedral sites of symmetry in the LX_6^{3-} anions, so that threefold vibrational and electronic degeneracies may be retained, thereby, in principle, providing relatively simple vibrational and electronic spectra. The Raman spectra thus exhibit only four bands, due to $\mathbf{k}=0$ vibrational modes of the crystal, but at low temperatures some additional features may be resolved which correspond to electronic Raman bands.

The aim of the present work was to extend the previous studies[1,2] in a quantitative manner by investigating the agreement between theory and experiment for the intensities of electronic Raman bands. The Judd-Ofelt-Axe theory employed is outlined in Sec. III, and some of the more detailed account[3] of the theory of Raman spectroscopy is also quoted in Sec. IV H for discussion. The relative intensity—excitation line dependence of the electronic Raman bands of $Cs_2NaTmCl_6$ at 120 K has been investigated, including the case when the excitation (476.5 nm) corresponded to $4f^n - 4f^n$ electron transition energies, so that the so-called resonant Raman scattering occurred. Moreover, a preliminary study has been made of the coupling between electronic crystal-field states and phonon states in the electronic ground-state multiplets of two elpasolite systems. Finally, studies of the Raman spectra of mixed crystals are referred to in Sec. V.

Some key studies of electronic Raman and resonance Raman spectroscopy have focused on the electron-phonon coupling in rare-earth vanadates[4] and phosphates,[5–7] on asymmetry and absolute electronic Raman-scattering cross sections for $4f^n - 4f^n$ transitions,[8,9] on resonance electronic Raman scattering,[10,11] and on the Judd-Ofelt-Axe (JOA) closure approximation calculation.[12] We briefly review some of the results from these studies which are relevant to the present work.

The electronic Raman-scattering intensity ratios for transitions from the ground state to the crystal-field levels of the $^4I_{15/2}$ multiplet of Er^{3+} in $ErPO_4$ were calculated by Becker, based upon JOA theory.[12] The predicted intensity was found to be in closer agreement with experiment when the ratio of the scattering parameters F_1/F_2 [Sec. III, Eq. (4)] was adjusted to a rather lower value than estimated by theory. To-

gether with electronic Raman data from $TmPO_4$ and $HoPO_4$ the low ratio was interpreted as showing the involvement of $4f^{n-1}5g^1$ electron configuration intermediate states in the electronic Raman spectra of these systems. Although the calculated electronic Raman-scattering intensity ratios for $CePO_4$ were in reasonable agreement with experiment, it was found that the application of standard JOA theory was particularly inadequate for electronic Raman-scattering in $TmPO_4$.[12] A subsequent *direct* calculation of the electronic Raman-scattering intensities in $TmPO_4$ included the detailed energy-level structure of the intermediate excited configuration, $4f^{11}5d^1$ and gave improved results.[8] However, significant differences remained, notably the absence of two electronic lines near 250 cm^{-1} in the spectrum. Xia[5] interpreted this discrepancy by a mechanism in which the excited states undergo fast nonradiative decay into two optical phonons. We also make similar interpretations in the present discussion.

An investigation of the electronic and vibrational Raman spectra of $YbPO_4$ revealed the occurrence of a temperature-dependent electron-phonon coupling with a coupling strength about an order of magnitude greater than previously reported.[6] The observations were interpreted under a model in which the off-diagonal electron-phonon interaction element was related to the electronic ground-state population factor.[6] It turns out that a similar phenomenom is observed in the present study of Cs_2NaLCl_6 not only for $L=$Yb but also Tm. A preliminary account of the electron-phonon coupling, which is different from the mechanism in Ref. 6, is given here and a more general discussion of this phenomenom will be presented elsewhere.

Williams *et al.* investigated the electronic Raman scattering of Ce^{3+} in $LuPO_4$ and observed intensity enhancements of the order of 10^2 when the laser excitation was tuned close to the energy of the $5d^1$ configuration.[11] The results were generally in agreement with that expected for electronic Raman scattering in which the states of the $5d^1$ configuration act as the intermediate states. In addition, the enhancements of the intensities of electronic Raman transitions were found to be of the order of 10^2 under resonant excitation to an energy level within the configuration $4f^{11}$ of Er^{3+} in $ErPO_4$.[10] In the present study of resonance scattering for $Cs_2NaTmCl_6$, the excitation is also within the configuration $4f^{12}$ but the enhancement mechanism must differ because there are no odd-parity static crystal-field components at the lanthanide ion site in the elpasolite lattice. We describe this unusual mechanism in Sec. IV H.

II. EXPERIMENT

Hexachloroelpasolite crystals were prepared in sealed quartz tubes from lanthanide oxides (99.9–99.999%, Strem Chemicals) by passing the residue from Morss method E[13] through a Bridgmann furnace. Raman spectra were recorded at a resolution of $1-2$ cm^{-1} using a Spex 1403-DM spectrometer equipped with a liquid-nitrogen cryostat and an Oxford Instruments closed-cycle cooler cryostat. Perpendicular faces were polished onto a crystal of $Cs_2NaYbCl_6$ and although the 300-K polarized Raman spectrum permitted the identification of the ν_1 totally symmetric mode, the experiments demonstrated that samples were polycrystalline. (The nontotally symmetric contributions[3] to ν_1 scattering were found to be negligible.) Electronic Raman-scattering intensities were measured relative to a suitable well-resolved electronic Raman transition of appropriate intensity by integration of the peak areas. The comparison with the intensity of vibrational Raman scattering was also made from the integration of the ν_1 peak area. The main error in peak area measurement was the choice of baseline, particularly where overlap occurred, and an indication of precision has been included in our experimental results (Table I).

Several additional bands were observed in the 488-nm excited 20 K Raman spectrum of $Cs_2NaYbCl_6$, compared with other argon-ion excitation lines. This excitation energy coincides with the cooperative absorption of two $YbCl_6^{3-}$ ions. However the concentration dependence of the bands showed that they were not due to cooperative emission but rather to an unidentified impurity.

III. CALCULATION OF ELECTRONIC RAMAN-SCATTERING INTENSITY RATIOS

Theoretically, when the polarizations of an incident photon $\hbar\omega$ and a scattering photon $\hbar\omega_s$ are σ and ρ, respectively, the electronic Raman-scattering amplitude from vibronic state $|i\rangle$ to $|f\rangle$ (where the phonon states in $|i\rangle$ and $|f\rangle$ are the same, and both are usually zero-phonon states) can be written as $\langle f|\alpha_{\rho\sigma}|i\rangle$. The Cartesian electronic Raman-scattering tensor is written as[3A]

$$\alpha_{\rho\sigma}=-\sum_r\left[\frac{D_\rho|r\rangle\langle r|D_\sigma}{\hbar\omega_r-\hbar\omega}+\frac{D_\sigma|r\rangle\langle r|D_\rho}{\hbar\omega_r+\hbar\omega_s}\right], \tag{1}$$

where D is the electric dipole operator and $|r\rangle$ is an intermediate vibronic state with electronic parity opposite to the one of $|i\rangle$ and $|f\rangle$. In the present case, where $|i\rangle$ and $|f\rangle$ are vibronic states of electronic configuration $4f^n$, $|r\rangle$ is taken to be a vibronic state of the configuration such as $4f^{n-1}5d^1$ and $4f^{n-1}5g^1$. According to theory of electronic structure of lanthanide ions the Cartesian tensor $\alpha_{\rho\sigma}$ is usually turned into a linear combination of spherical tensors $\alpha_q^{(t)}$:

$$\alpha_{\rho\sigma}=\sum_{t,q}C_{\rho\sigma}^{tq}\alpha_q^{(t)}, \tag{2}$$

where $t=0,1,2$. The coefficients $C_{\rho\sigma}^{tq}$ can be calculated in the usual way or taken from Ref. 3B, and determine the irreducible spherical tensor composition of the polarization component $\alpha_{\rho\sigma}$ of the Cartesian scattering matrix $[\alpha_{\rho\sigma}]$. The spherical tensor

$$\alpha_q^{(t)}\approx U_q^{(t)}F_t, \tag{3}$$

in which $U_q^{(t)}$ is a unit tensor acting on the electronic wave functions $\langle f|$ and $|i\rangle$ within the configuration of $4f^n$. F_t is the following scattering parameter independent of $\langle f|$ and $|i\rangle$, and is obtained from the Judd-Ofelt-Axe theory by invoking the closure approximation:[14]

TABLE I. Assignment and intensities of electronic Raman transitions of Cs_2NaLCl_6. n.o.: not observed; w: weak; vw: very weak. Values in parentheses are taken from electronic spectra (Ref. 16). The chosen F_1 and F_2 values are representative and not best fit.

		Electronic Raman transition Relative intensity			
L	Energy (cm^{-1})	Obs.	Theor.	Calc.	Assignment
				$F_1=0.00$	
				$F_2=4.13$	
Ce	562,580	4.18 ± 0.45	$0.2449\|F_2\|^2+0.2073\|F_1\|^2$	4.18	$(^2F_{5/2})\Gamma_7\rightarrow\Gamma_8(^2F_{5/2})$
	2161	0.16 ± 0.01	$0.0078\|F_1\|^2$	0.00	$(^2F_{5/2})\Gamma_7\rightarrow\Gamma_7(^2F_{7/2})$
	2663	0.86 ± 0.07	$0.0227\|F_2\|^2+0.0058\|F_1\|^2$	0.39	$(^2F_{5/2})\Gamma_7\rightarrow\Gamma_8(^2F_{7/2})$
	3050	1.00	$0.0181\|F_2\|^2$	0.31	$(^2F_{5/2})\Gamma_7\rightarrow\Gamma_6(^2F_{7/2})$
	280	1.0 ± 0.3			ν_1
				$F_1=1.96$	
				$F_2=6.26$	
Pr	234,250	1.23 ± 0.01	$0.3217\|F_1\|^2$	1.23	$(^3H_4)\Gamma_1\rightarrow\Gamma_4(^3H_4)$
	416,428	0.19 ± 0.04	$0.0647\|F_2\|^2$	2.53	$(^3H_4)\Gamma_1\rightarrow\Gamma_3(^3H_4)$
	704	1.00	$0.0255\|F_2\|^2$	1.00	$(^3H_4)\Gamma_1\rightarrow\Gamma_5(^3H_4)$
	(2300)	n.o.	$0.0026\|F_1\|^2$	0.01	$(^3H_4)\Gamma_1\rightarrow a\Gamma_4(^3H_5)$
	2400	0.24 ± 0.08	$0.0060\|F_2\|^2$	0.24	$(^3H_4)\Gamma_1\rightarrow\Gamma_5(^3H_5)$
	(2643)	n.o.	$0.0007\|F_2\|^2$	0.03	$(^3H_4)\Gamma_1\rightarrow\Gamma_3(^3H_5)$
	(4392)	n.o.	$0.0006\|F_2\|^2$	0.02	$(^3H_4)\Gamma_1\rightarrow\Gamma_3(^3H_6)$
	(4437)	n.o.	$0.0000\|F_2\|^2$	0.00	$(^3H_4)\Gamma_1\rightarrow a\Gamma_5(^3H_6)$
	(4878)	n.o.	$0.0044\|F_2\|^2$	0.17	$(^3H_4)\Gamma_1\rightarrow b\Gamma_5(^3H_6)$
	5205	vw	$0.0315\|F_2\|^2$	1.23	$(^3H_4)\Gamma_1\rightarrow\Gamma_3(^3F_2)$
	(5294)	n.o. [a]	$0.0175\|F_2\|^2$	0.69	$(^3H_4)\Gamma_1\rightarrow\Gamma_5(^3F_2)$
	(6613)	n.o.	$0.0000\|F_1\|^2$	0.00	$(^3H_4)\Gamma_1\rightarrow\Gamma_4(^3F_3)$
	6622	w	$0.0075\|F_2\|^2$	0.29	$(^3H_4)\Gamma_1\rightarrow\Gamma_5(^3F_3)$
	(6964)	n.o.			$(^3H_4)\Gamma_1\rightarrow\Gamma_3(^3\Gamma_4)$
	280	1.5 ± 0.4			ν_1
				$F_1=0.99$	
				$F_2=5.78$	
Eu	360	0.14 ± 0.04	$0.1429\|F_1\|^2$	0.14	$(^7F_0)\Gamma_1\rightarrow\Gamma_4(^7F_1)$
	875	4.7 ± 0.5	$0.0571\|F_2\|^2$	1.91	$(^7F_0)\Gamma_1\rightarrow\Gamma_3(^7F_2)$
	1091	1.00	$0.0857\|F_2\|^2$	2.90	$(^7F_0)\Gamma_1\rightarrow\Gamma_5(^7F_2)$
	290	2.5 ± 0.3			ν_1
Er [b]	25	0.8 ± 0.4			$(^4I_{15/2})a\Gamma_8\rightarrow\Gamma_7(^4I_{15/2})$
	56	1.00			$(^4I_{15/2})a\Gamma_8\rightarrow b\Gamma_8(^4I_{15/2})$
	(259)	n.o.			$(^4I_{15/2})a\Gamma_8\rightarrow\Gamma_6(^4I_{15/2})$
	296	14 ± 1			ν_1
Tm at 120 K under 476.5 nm excitation [c]					
	56	n.o.	$0.3477\|F_1\|^2$		$(^3H_6)\Gamma_1\rightarrow\Gamma_4(^3H_6)$
	68	4 ± 1	$0.0102\|F_2\|^2+0.5433\|F_1\|^2$		$(^3H_6)\Gamma_4\rightarrow a\Gamma_5(^3H_6)$
	200	1.00	$0.1152\|F_2\|^2$		$(^3H_6)\Gamma_4\rightarrow\Gamma_2(^3H_6)$
	(314)	n.o.	$0.0711\|F_2\|^2+0.0786\|F_1\|^2$		$(^3H_6)\Gamma_4\rightarrow b\Gamma_5(^3H_6)$
	(338)	n.o.	$0.0012\|F_2\|^2+0.0498\|F_1\|^2$		$(^3H_6)\Gamma_4\rightarrow\Gamma_3(^3H_6)$
	294	15 ± 3			ν_1
Tm at 20 K [d]					
	56	n.o.	$0.3477\|F_1\|^2$		$(^3H_6)\Gamma_1\rightarrow\Gamma_4(^3H_6)$
	108 [e]	1.00	$0.0743\|F_2\|^2$		$(^3H_6)\Gamma_1\rightarrow a\Gamma_5^c(^3H_6)$
	148 [e]	2.23 ± 0.05			$(^3H_6)\Gamma_1\rightarrow a\Gamma_5^{c'}(^3H_6)$
	(370)	n.o.	$0.0140\|F_2\|^2$		$(^3H_6)\Gamma_1\rightarrow b\Gamma_5(^3H_6)$

TABLE I. (*Continued*).

		Electronic Raman transition Relative intensity			
L	Energy (cm^{-1})	Obs.	Theor.	Calc.	Assignment
	(394)	n.o.	$0.0051\|F_2\|^2$		$(^3H_6)\Gamma_1\rightarrow\Gamma_3(^3H_6)$
	297	0.75 ± 0.06			ν_1
				$F_1=1.47$	
				$F_2=1.82$	
Yb	203 [e]	1.00	$0.1701\|F_2\|^2+0.2041\|F_1\|^2$	1.00	$(^2F_{7/2})\Gamma_6\rightarrow\Gamma_8^d(^2F_{7/2})$
	572	0.28 ± 0.04	$0.0850\|F_2\|^2$	0.28	$(^2F_{7/2})\Gamma_6\rightarrow\Gamma_7(^2F_{7/2})$
	294	2.32 ± 0.03			ν_1

[a]Feature reported at 5297 cm^{-1} in Ref. 1.

[b]Calculations were not performed. Resonance enhancement occurs when under 496.5 nm excitation.

[c]Resonant enhancement occurs notably for transitions from $(^3H_6)\Gamma_4$. There is insufficient data to fit F_1 and F_2.

[d]Strong electron-phonon coupling effects are observed so that the fits to F_1 and F_2 have not been made. The coupled modes are denoted by (e).

$$F_t=(-1)^t\sum_{n'l'}7(2l'+1)\begin{pmatrix}3&1&l'\\0&0&0\end{pmatrix}^2\times\langle 4f|r|n'l'\rangle^2(2t+1)^{1/2}\begin{Bmatrix}1&3&l'\\3&1&t\end{Bmatrix}EN, \quad (4a)$$

where

$$EN=\left\{\frac{1}{E(n'l')-\hbar\omega}+\frac{(-1)^t}{E(n'l')+\hbar\omega}\right\}, \quad (4b)$$

where $(n'l')$ represents the intermediate electronic configuration $4f^{n-1}(n'l')^1$ having opposite parity to $4f^n$, and having an average energy $E(n'l')$ higher than that of the ground state. Thus, besides $\langle 4f|r|5d\rangle$, the parameter F_t is determined by the energy structure of the intermediate configurations $n'l'$, and from these configurations the $4f^{n-1}5d$ is lowest in energy and is the most important one in the summation (4). If F_t is entirely contributed by $5d^1$, the ratio

$$F_1/F_2=1.3[\hbar\omega/E(5d)], \quad (5)$$

based on Eq. (4).

Considering the O_h molecular point-group site symmetry of L^{3+} in a microcrystal Cs_2NaLCl_6 the matrix $[\alpha_{\rho\sigma}]$ can be split into nine matrices belonging to four irreps Γ_α ($\alpha=1,3,4,5$) of group O_h. Of these, Γ_1 is constructed only by $\alpha_0^{(0)}$ representing Rayleigh scattering, and Γ_4 only by $\alpha_q^{(1)}$ and is antisymmetric ($C_{\rho\sigma}^{1q}=-C_{\sigma\rho}^{1q}$). Similarly, $|i\rangle$ and $|f\rangle$ also form bases (Γ_i and Γ_f, respectively) of the O_h molecular point group, and the selection rule for electronic Raman scattering $i\rightarrow f$ takes the form:

$$\Gamma_f\otimes\Gamma_i\subset\Gamma_\alpha. \quad (6)$$

In the present study the samples used were polycrystalline, so for a $\hbar\omega\rightarrow\hbar\omega_s$ scattering intensities contributed by various polarization components $\alpha_{\rho\sigma}$ should be summed incoherently, i.e., $\Sigma_{\rho\sigma}|\langle f|\alpha_{\rho\sigma}|i\rangle|^2$ was calculated. Since $\alpha_{\rho\sigma}$ has all of the terms on the right-hand side of Eq. (2), the squared elements $|\langle f|\alpha_{\rho\sigma}|i\rangle|^2$ contain coherent contributions from different scattering spherical tensors $\alpha_q^{(t)}$. However, we find that all of these coherent terms disappeared after the summation over ρ and σ, which is expected since for a polycrystalline sample only the incoherent terms remain. In addition, usually the levels E_i and E_f are degenerate (i.e., the initial and final states $|i\rangle$ and $|f\rangle$ are $|\Gamma_i\gamma_i\rangle$ and $|\Gamma_f\gamma_f\rangle$, respectively) so that the scattering intensities of all transitions from various $|\Gamma_i\gamma_i\rangle$ to various $|\Gamma_f\gamma_f\rangle$ for a $\hbar\omega\rightarrow\hbar\omega_s$ scattering (corresponding to $\Gamma_i\rightarrow\Gamma_f$) need to be summed incoherently, i.e., $\Sigma_{\rho\sigma\gamma_i\gamma_f}|\langle\Gamma_f\gamma_f|\alpha_{\rho\sigma}|\Gamma_i\gamma_i\rangle|^2$ is calculated. As expected this always equals $m_i\Sigma_{\rho\sigma\gamma_f}|\langle\Gamma_f\gamma_f|\alpha_{\rho\sigma}|\Gamma_i\gamma_i\rangle|^2$, where m_i is the degree of degeneracy of the initial state $|\Gamma_i\gamma_i\rangle$.

IV. RESULTS AND DISCUSSION

A. Vibrational Raman scattering

A unit-cell-group analysis[15] of the Cs_2NaLCl_6 elpasolite system provides the following Raman-active modes of vibration:

$$\Gamma(\text{vib.:Raman})\subset\nu_1(\alpha_{1g});\nu_2(\epsilon_g);\nu_5(\tau_{2g});l(\tau_{2g}), \quad (7)$$

where the labels of the LCl_6^{3-} moeity modes, ν_i, $i=1-5$, refer to irreducible representations of the O_h point group, and l is a caesium translatory lattice mode.

Figure 1(a) shows the energies of the internal vibrational modes ν_1, ν_2, and ν_5 in the 20-K Raman spectra of the elpasolites Cs_2NaLCl_6. In each case, the energies show an overall increase with the number of f electrons in the L^{3+} cation. Figure 1(b) compares the integrated intensity ratios of the vibrational Raman bands $I(\nu_2/\nu_1)$ and $I(\nu_5/\nu_1)$ for Cs_2NaLCl_6 at low temperature. The ratios both show an overall decrease with increasing number of f electrons in L^{3+}. The intensity ratios exhibit a similar trend at room temperature but the values are larger, particularly for $I(\nu_5/\nu_1)$. Obviously, the larger intensity ratio arises from the increase with temperature of the factors $(\overline{n_2}+1)/(\overline{n_1}+1)$ in $I(\nu_2/\nu_1)$, and $(\overline{n_5}+1)/(\overline{n_1}+1)$ in $I(\nu_5/\nu_1)$, since

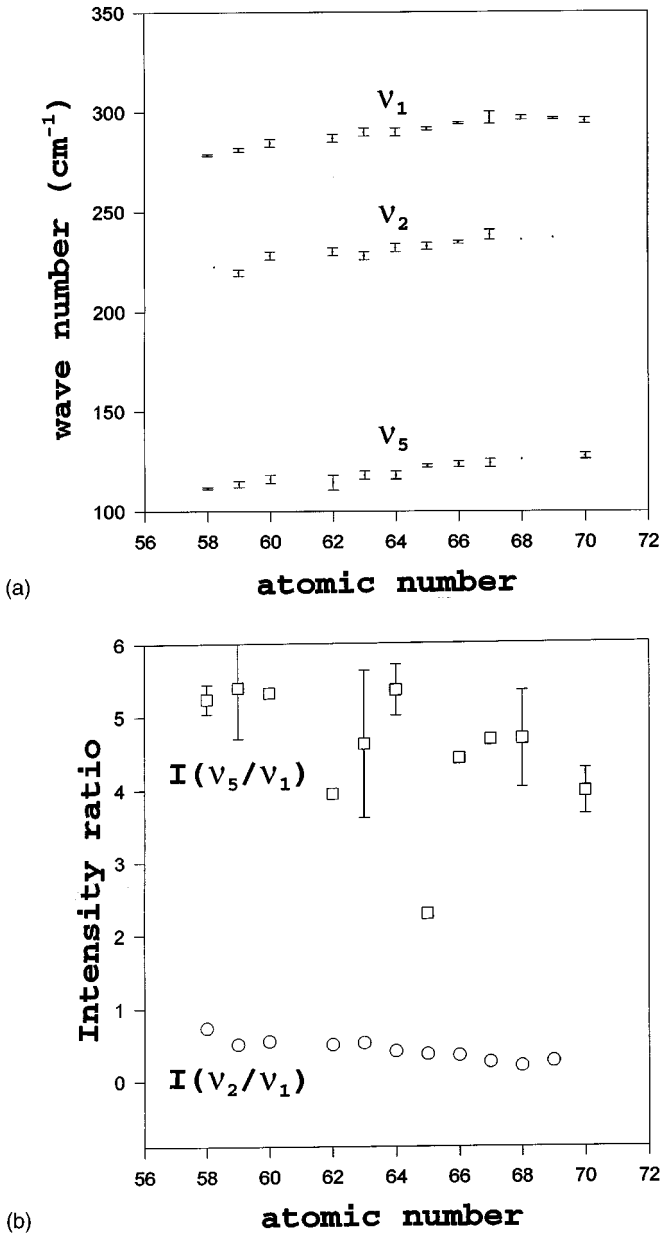

FIG. 1. Plots of the atomic number of L as a function of (a) the energies of the ν_1, ν_2, and ν_5 internal modes (b) the integrated intensity ratios of ν_2/ν_1 and ν_5/ν_1 from the 20 K vibrational Raman spectra of Cs_2NaLCl_6. Data points are mean values from this study and from Refs. 1 and 2. Error bars reflect the differences between values from this study and from Ref. 1, single points indicating agreement; otherwise an error of $\pm 2\ cm^{-1}$ has been taken for energy measurements. The linear regression equations for (a) are $\nu_1 = 190.89 + 1.55Z$, $(R = 0.962)$; $\nu_2 = 132.70 + 1.54Z$, $(R = 0.937)$; $\nu_5 = 31.86 + 1.37Z$, $(R = 0.968)$.

the average occupation number $\overline{n_\nu}$ of phonons is proportional to $\exp(-h\nu/kT)$ at temperature T, and $120\ cm^{-1} \approx h\nu_5 < h\nu_2 < h\nu_1 \approx 290\ cm^{-1}$.

B. Electronic Raman scattering

In some cases, the low-temperature Raman spectra of Cs_2NaLCl_6 exhibit additional features to the vibrational Raman bands. These features sharpen on cooling, and the energies are found to correspond to those of the crystal-field levels of the respective multiplet terms, as identified from absorption, excitation, and luminescence spectroscopy.[16] In this section, the electronic Raman bands are discussed for each lanthanide ion in turn, and their relative intensities are compared with calculation. The lanthanide ions L = Ce-Eu in Cs_2NaLCl_6 undergo phase transitions between 90 and 180 K to a tetragonal form.[17] The splittings due to the removal of vibrational degeneracies of the τ_{2g} and ϵ_g modes are not resolved in the Raman spectra, but the site symmetry perturbation results in splittings of up to $20\ cm^{-1}$ for electronic crystal-field levels.[16] The perturbation from O_h site symmetry is neglected in the present study since the integrated intensity ratios of the electronic Raman bands were found to be similar at temperatures above and below the phase transitions. The energies and wave functions of the electronic states of Cs_2NaLCl_6 relevant to the present study, as determined from absorption, excitation, and emission spectra, are listed in Appendix A, and these have been utilized in the electronic Raman intensity calculations. The electronic Raman transitions of Cs_2NaLCl_6 are assigned in Table I, and the scattering intensity ratios are listed and compared with the calculated values. For each compound the relative intensity of the vibrational ν_1 band is also included for reference. The ratio F_1/F_2 is compared in Sec. VI for the different lanthanide ions doped into the elpasolite host lattice.

C. Electronic Raman scattering of $Cs_2NaCeCl_6$

Figure 2(a) shows the low-energy part of the Raman spectrum of $Cs_2NaCeCl_6$ at 80 and 20 K. The electronic ground state is $(^2F_{5/2})\Gamma_7$, with the $(^2F_{5/2})\Gamma_8$ level calculated[16] to be at $570\ cm^{-1}$. The three crystal-field levels of the next highest multiplet term, $^2F_{7/2}$, are calculated between 2160 and $3048\ cm^{-1}$. The electronic Raman transitions from the ground state to all these excited states are allowed by selection rules.

The electronic Raman transition to the Γ_8 level is observed near $570\ cm^{-1}$ at 80 K, but split into two components at 20 K [Fig. 2(a)]. Three higher energy bands are observed which correspond to the $(^2F_{5/2})\Gamma_7 \rightarrow \Gamma_6, \Gamma_8, \Gamma_7(^2F_{7/2})$ transitions (Table I). These observations are in agreement with those of Amberger, Rosenbauer, and Fischer.[18] Comparing the observed and theoretical relative intensities (Table I), it is apparent that the magnitude of the parameter F_1 does not play a significant role in accounting for the observed values. When set to zero (Table I) the calculated relative intensities are not very different from the observed ones. However, when the ratio F_1/F_2 is set to the theoretical value [0.68, from Eq. (4), since $E(5d)$ is measured from available absorption spectral data[19] for $Cs_2NaYCl_6:Ce^{3+}$ to be $37\ 165\ cm^{-1}$], the values of F_1 and F_2 become 2.38 and 3.50. The agreement with the observed intensities, relative to the bands near $570\ cm^{-1}$, is satisfactory for the $\Gamma_7 \rightarrow \Gamma_7(^2F_{7/2})$ transition, but the relative intensities of the transitions to the Γ_8 and $\Gamma_6(^2F_{7/2})$ crystal-field levels are calculated to be smaller (0.31 and 0.22, respectively).

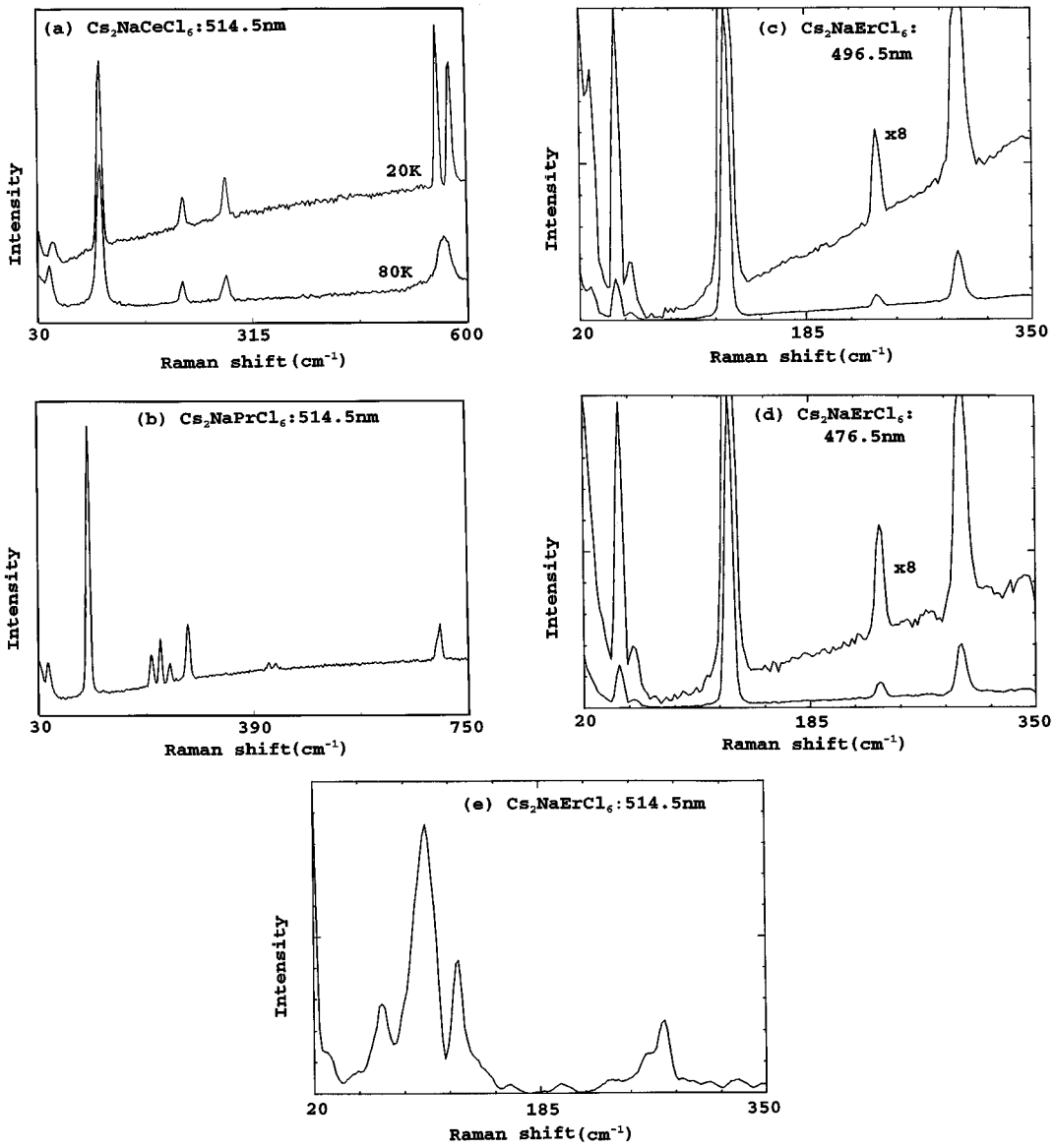

FIG. 2. Raman spectra of Cs_2NaLCl_6: 514.5 nm excited spectrum of (a) $Cs_2NaCeCl_6$ at 80 K and 20 K; (b) $Cs_2NaPrCl_6$ at 20 K; spectra of $Cs_2NaErCl_6$ at 20 K using (c) 496.5 nm, (d) 476.5 nm, and (e) 514.5 nm excitation.

D. Electronic Raman scattering of $Cs_2NaPrCl_6$

Part of the 20-K spectrum of $Cs_2NaPrCl_6$ is shown in Fig. 2(b). Transitions are observed not only from the $(^3H_4)\Gamma_1$ ground state to the excited crystal-field levels of the ground multiplet $^3H_4$, but also to several excited multiplets, in order of increasing energy: $^3H_5$, $^3F_2$, and $^3F_3$. The derived wave numbers of the terminal states are in agreement with those from infrared absorption and optical emission spectroscopy.[16] The spectrum is interesting because the strongest electronic Raman bands (near 234, 250 cm^{-1}) are governed by the antisymmetric tensor (as are the unobserved transitions at 2300 and 6613 cm^{-1}). The electronic Raman transitions to the $(^3H_4)\Gamma_3$ levels near 420 cm^{-1} are weak. Under 514.5-nm excitation, the transitions to $^3H_5$ are superimposed upon absorption bands due to the $^3H_4 \rightarrow {}^1D_2$ transition, and only the electronic Raman transition to $(^3H_5)\Gamma_5$ is located. Transitions to $^3H_6$ crystal-field levels are too weak to be observed, whereas the single features observed for transitions to the $^3F_2$ and $^3F_3$ terms enable the identifications of the representations of the terminal states to be made. We do not observe the bands reported by Amberger, Rosenbauer, and Fischer[1] at 4936, 5005, and 5297 cm^{-1}. The first two energies of these bands cannot be rationalized from the energy-level scheme of Pr^{3+} in $Cs_2NaPrCl_6$.[16] The feature reported at 5297 cm^{-1} most likely corresponds to the electronic Raman transition from the ground state to $(^3F_2)\Gamma_5$, this level being located from infrared spectra at 5294 cm^{-1}. This band is obscured by noise in our spectra and is calculated to be about half as intense as the electronic Raman band at 5205 cm^{-1} which we observe to be very weak.

By setting $F_1 = 1.96$ and $F_2 = 6.26$, the calculated intensities are in reasonable agreement with experiment (especially when Amberger's observation is considered) except for the intensities at 416 and 428 cm^{-1}. This means that the

JOA closure approximation works well here, and the large value (0.31) of F_1/F_2 provides evidence that the $4f^15d^1$ configuration contributes almost to be the only intermediate configuration, and $E(5d) \cong 80\,000\ \mathrm{cm}^{-1}$. The experimental low intensities of the bands at 416 and 428 cm^{-1} may be rationalized by the small excited-state lifetimes due to the two (218 cm^{-1}) ϵ_g phonon decay of these states to Γ_1, and/or the two (96 cm^{-1}) τ_{1u} phonon decay to Γ_4.

E. Electronic Raman scattering of $Cs_2NaEuCl_6$

The electronic Raman spectrum of $Cs_2NaEuCl_6$ has been previously reported.[20] Electronic Raman bands overlap emission bands at 120 K, so that the choice of baseline is uncertain for intensity measurements. However, the relative intensities of electronic Raman bands differ considerably, with $^7F_0 \rightarrow {}^7F_2$ being much stronger than $^7F_0 \rightarrow {}^7F_1$. Theoretically, they are determined by the parameters F_2 and F_1 respectively, so this observation is readily understood (Table I). The relative intensities of the two $^7F_0 \rightarrow {}^7F_2$ transitions differ considerably, however, for theory and experiment. The theoretical intensities are proportional to the degeneracy degree of the terminal crystal-field states. The experimental ratios were measured for several different excitation lines. The discrepancy could arise from the use of the JOA model and/or from the tetragonal site symmetry perturbation. Alternatively, the weak intensity of the $\Gamma_1 \rightarrow \Gamma_5$ transition may be attributed to the decay of the Γ_5 state by two τ_{2g} phonons to populate Γ_3. Two $^7F_0 \rightarrow {}^7F_3$ transitions reported by Amberger, Rosenbauer, and Fischer[1] are obscured by luminescence under the excitation used in the present study.

F. Electronic Raman scattering of $Cs_2NaErCl_6$

The ground-state term of Er^{3+} is $^4I_{15/2}$ and the next highest term, $^4I_{13/2}$ is about 6000 cm^{-1} to high energy. Electronic Raman transitions are expected from the $(^4I_{15/2})\Gamma_8$ ground state to the other crystal-field levels of $^4I_{15/2}$, Amberger, Rosenbauer, and Fischer[1] reported one electronic Raman transition at 56 cm^{-1}.

Figures 2(c)–(e) show the 20 K spectra of $Cs_2NaErCl_6$ under different argon-ion excitation lines. The crystal is transparent to 476.5 nm [20 981 cm^{-1}, Fig. 2(d)] and 496.5 nm [20 135 cm^{-1}, Fig. 2(c)] radiation, and the vibrational Raman bands are accompanied by two bands near 25 and 56 cm^{-1} in both cases, which correspond to the $(^4I_{15/2})a\Gamma_8 \rightarrow \Gamma_7(^4I_{15/2})$ and $b\Gamma_8(^4I_{15/2})$ electronic Raman transitions, respectively. It is clear from Figs. 2(c) and 2(d) that the intensity of the two electronic Raman bands is slightly greater, relative to the ν_2 vibration, under 496.5 nm excitation than under 476.5 nm excitation. We do not present quantitative data herein and will reinvestigate this phenomenon using dye-laser excitation. This former excitation energy (20 135 cm^{-1}) lies nearer in energy to the spectral bands in the vibrational sideband of the $^4I_{15/2} \rightarrow {}^4F_{7/2}$ transition of $Cs_2NaErCl_6$.[16] A small resonant enhancement of the electronic Raman transition is therefore observed when the intermediate state is $(^4F_{7/2}) + \nu_{\mathrm{odd}}$, where ν_{odd} refers to an odd-parity internal vibration of $Cs_2NaErCl_6$, and the mechanism is discussed in Sec. IV H.

Excitation using the 514.5 nm argon-ion excitation line results in emission. This radiation is strongly absorbed by the vibronic sideband of the $^4I_{15/2} \rightarrow {}^2H_{11/2}$ transition and upconversion occurs to ultraviolet levels,[21] from which emission occurs. Figure 2(e) shows the spectrum under this excitation line, with the characteristic vibronic ν_3, ν_4, ν_6 sidebands of $ErCl_6^{3-}$ (see Ref. 21). The (unobserved) zero-phonon line inferred to be at 19 414 cm^{-1}, so that this transition corresponds to $(^4G_{11/2})\Gamma_8 \rightarrow \Gamma_8, \Gamma_7(^4I_{13/2})$.[21]

Williams *et al.*[10] were able to probe the resonant Raman scattering of $ErPO_4$ under blue-green excitation without the complications of emission. Indeed, it was carefully demonstrated that the spectral bands corresponded to scattering and not emission. The reason for the absence of emission is clear from the energy-level scheme of $ErPO_4$, several resonant ion-ion cross relaxations leading to depopulation of the lowest $^4F_{7/2}$ level, Γ_6, in this host. The different energy-level structure of the elpasolite $Cs_2NaErCl_6$ does not provide a resonant transfer pathway and weak emission is observed from $^4F_{7/2}$ in the elpasolite lattice.

G. Electronic Raman scattering of $Cs_2NaTmCl_6$

The study of the electronic Raman spectrum of $Cs_2NaTmCl_6$ is of interest for several reasons. First, the calculated crystal-field levels of the ground-state multiplet term show poor agreement with the experimental values from emission spectroscopy.[22] Second, this system provides the opportunity to probe the change in relative intensities of electronic Raman transitions when the Raman excitation is tuned through an intraconfigurational $4f^n - 4f^n$ transition, $^1G_4 \leftarrow {}^3H_6$. The luminescence from the $^1G_4$ state is quenched by a cross relaxation to the lower energy $^3H_4$ term multiplet[23] so that it does not obscure the Raman spectrum. Lastly, the Raman spectrum exhibits a marked change with temperature which is attributed to the effects of electron-phonon coupling.

H. Excited-state resonance electronic Raman scattering of $Cs_2NaTmCl_6$

The electronic ground state of Tm^{3+} is $(^3H_6)\Gamma_1$, with the crystal-field components of $^3H_6$ extending up to 394 cm^{-1}. Under argon-ion laser excitation, four vibrational Raman bands are observed in the room-temperature Raman spectrum of $Cs_2NaTmCl_6$ [Fig. 3(b)], corresponding to ν_l, ν_5, ν_2, and ν_1 in order of increasing energy. At 120 K some additional features are apparent [Figs. 3(b) and 3(c)]. Two of these bands, at 68 and 200 cm^{-1}, are assigned to hot electronic Raman transitions from the first excited state (Γ_4 at 56 cm^{-1}) to further excited electronic states which are deduced to be at 124 cm^{-1} ($a\Gamma_5$) and 256 cm^{-1} (Γ_2). These bands disappear at lower temperatures because the occupation of the initial state becomes negligible. Moreover, Fig. 3(c) clearly shows that the hot electronic Raman transitions appear strongest under 476.5-nm excitation. From the electronic absorption spectrum [Fig. 3(a)] which comprises the vibronic sidebands of the $^1G_4 \leftarrow (^3H_6)\Gamma_1$ transitions, it is evident that 476.5-nm (20 981 cm^{-1}) excitation coincides

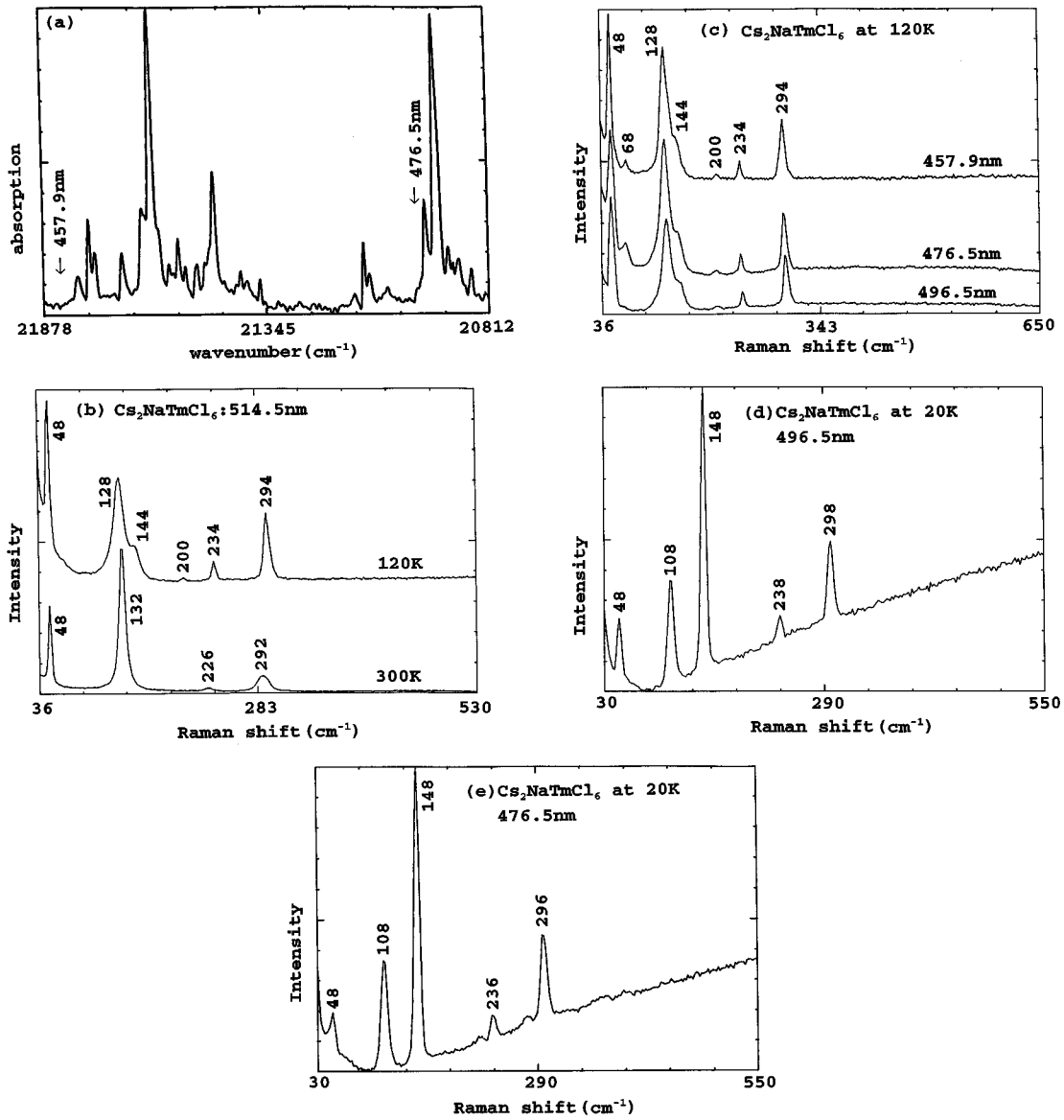

FIG. 3. Electronic absorption and Raman spectra of $Cs_2NaTmCl_6$: (a) 20 K electronic absorption spectrum recorded using single beam mode with Raman monochromators; (b) 514.5 nm excited Raman spectra at 300 and 120 K; (c) Raman spectra at 120 K using 457.9, 476.5, and 496.5 nm excitation; Raman spectra at 20 K using (d) 496.5 nm and (e) 476.5 nm excitation. Two additional weak, broadbands which are observed in (e) correspond to the strongest vibronic structure of the luminescence spectrum ($[^1G_4]\Gamma_5 \rightarrow [^3H_6]\Gamma_1 + \nu_6$, $[^3H_6]\Gamma_4 + \nu_6$).

with the tail of a vibronic origin, and 457.9-nm excitation lies at the edge of the absorption sideband. 496.5- and 514.5-nm excitation both do not coincide with absorption bands. However, excitation by 20 981 cm^{-1} from the first excited crystal-field level of $Cs_2NaTmCl_6$ (Γ_4 at 56 cm^{-1}) results in a stronger absorption hot band, $(^1G_4)\Gamma_5 + \nu_3 \leftarrow (^3H_6)\Gamma_4$, near 21 040 cm^{-1}. The enhanced intensity of the electronic Raman transitions originating from $(^3H_6)\Gamma_4$ under 476.5 nm excitation [Figs. 3(b), 3(c)] can therefore be attributed to the hot population of the Γ_4 level, and to the contribution from resonant electronic Raman scattering, which has not been considered in the JOA calculated intensities of transitions from the first excited state $(^3H_6)\Gamma_4$. We do not therefore provide values of F_1 and F_2 in this case (Table I: Tm at 120 K). The transition from the electronic ground state, $(^3H_6)\Gamma_1$ to the crystal-field level, $\Gamma_4(^3H_6)$ is too weak to be observed (Sec. IV I).

Clark and Dines[3] presented a simplified expression of $\langle f|\alpha_{\rho\sigma}|i\rangle$ by summation of the terms A, B, C, and D in formulas (19)–(22) therein to describe resonance Raman scattering. Starting from their formula (2) (which corresponds to Eq. (1) in this paper), by introducing the following adiabatic Born-Oppenheimer approximation of the vibronic states in the above scattering amplitude $\langle f|\alpha_{\rho\sigma}|i\rangle$:

$$|i\rangle = |gm\rangle \cong |g\rangle|m_g\rangle,$$
$$|f\rangle = |an\rangle \cong |a\rangle|n_a\rangle, \tag{8}$$
$$|r\rangle = |ev\rangle \cong |e\rangle|v_e\rangle,$$

where $|g\rangle$, $|a\rangle$, and $|e\rangle$ are initial, final, and intermediate (here, resonant) electronic states and $|m_g\rangle$, $|n_a\rangle$, and $|v_e\rangle$ are the corresponding harmonic vibrational states, respectively. Including the electron-phonon coupling Hamiltonian:

$$H' = \sum_k \left|\frac{\partial H}{\partial Q_k}\right|_{Q'_s=0} Q_k, \tag{9}$$

where Q_k is the normal coordinate of the kth vibrational mode of the system, we obtain the following corrected electronic states:

$$|e\rangle \Rightarrow |e\rangle + \sum_{e'(\neq e),k}{}' |e'\rangle \frac{h^k_{e'e}}{\hbar\omega_e - \hbar\omega_{e'}} Q_k, \tag{10}$$

where

$$h^k_{e'e} = \left\langle e' \left| \frac{\partial H}{\partial Q_k} \right| e \right\rangle \Bigg|_{Q'_s=0}. \tag{11}$$

Based on this and the resonance condition, Clark and Dines derived formulas (19)–(22) in Ref. 3, among which formula (19), i.e., the following A term (with $m_g = n_a = 0$) having no contribution from H' and (10):

$$A = [\mu_\rho]^0_{ae}[\mu_\sigma]^0_{eg} \sum_v \frac{\langle n_a|v_e\rangle\langle v_e|m_g\rangle}{[\hbar\omega_{ev} - \hbar\omega + i\Gamma_{ev}]}, \tag{12}$$

where

$$[\mu_\rho]^0_{ae} = \langle a|\mu_\rho|e\rangle, \tag{13}$$

and $i\Gamma_{ev}$ is a damping factor (in cm^{-1}) related to the lifetime of the state $|r\rangle = |ev\rangle$, was thought to be the dominant term of most resonance electronic Raman scatterings. It is really the case that the resonance scattering observed in $LuPO_4$:Ce^{3+} (Ref. 11) corresponds to $|e\rangle = |5d\rangle$, with large $[\mu_\rho]^0_{ae}$ and $[\mu_\sigma]^0_{eg}$; and the resonance observed in $ErPO_4$ (Ref. 10) corresponds to

$$|e\rangle = |(4f^n)\alpha\Gamma\gamma\rangle - \sum_\beta |(4f^{n-1}5d)\beta\Gamma\gamma\rangle \frac{\langle\beta|H''|\alpha\rangle}{\hbar\omega_\beta - \hbar\omega_\alpha}, \tag{14}$$

but both $[\mu_\rho]^0_{ae}$ and $[\mu_\sigma]^0_{eg}$ are very small since they are based on the perturbation-corrected terms in Eq. (14), which come from the matrix element $\langle\beta|H''|\alpha\rangle = \langle(4f^{n-1}5d)\beta\Gamma\gamma|H''|(4f^n)\alpha\Gamma\gamma\rangle$ of the static odd-parity crystal-field energy operator H''. However, the resonance scattering observed in the present study cannot be related to the above A term in Eq. (12) since for the L^{3+} ion in the elpasolite lattice there is no static odd-parity H'' so that $[\mu_\rho]^0_{ae}$ and $[\mu_\sigma]^0_{eg}$ in Eq. (12) are zero. Instead, the odd-parity terms contained in the electron-phonon coupling H' cause the corrected terms of $|e\rangle$ in Eq. (10), which can give nonzero $[\mu_\rho]^0_{ae''}$ and $[\mu_\sigma]^0_{e'g}$ instead of $[\mu_\rho]^0_{ae}$ and $[\mu_\sigma]^0_{eg}$. This result is equivalent to the so-called D terms [formula (22) in Ref. 3], with $m_g = n_a = 0$:

$$D = [\mu_\rho]^0_{ae''}[\mu_\sigma]^0_{e'g} \frac{h^k_{e''e} h^{k'}_{ee'}}{(\hbar\omega_{e''} - \hbar\omega_e)(\hbar\omega_{e'} - \hbar\omega_e)} \times \sum_v \frac{\langle n_a|Q_k|v_e\rangle\langle v_e|Q_{k'}|m_g\rangle}{(\hbar\omega_{ev} - \hbar\omega + i\Gamma_{ev})}. \tag{15}$$

The present report of the effects of this term in resonance electronic Raman scattering is therefore unusual.

I. Temperature-dependent electron-phonon coupling in $Cs_2NaTmCl_6$

It is very noticeable that instead of the τ_{2g} phonon peak near 132 cm^{-1} at room temperature, a band is observed near 144 cm^{-1} at 120 K, which becomes progressively stronger and changes to 148 cm^{-1} at 20 K. Furthermore, the ν_5 phonon band near 128 cm^{-1} at 120 K, disappears at 20 K, and another feature at 108 cm^{-1} is observed [Figs. 3(c)–3(e)]. This behavior is attributed to the interaction between the $a\Gamma_5$ electronic level and the $\Gamma_1 + \nu_5(\tau_{2g})$ vibronic level at low temperatures. We have found that the $\nu_5(\tau_{2g})$ energy decreases for the other solid-state hexachloroelpasolites by $4-5\ \mathrm{cm}^{-1}$ on cooling from 300 to 20 K. The (unperturbed) ν_5 energy in $Cs_2NaTmCl_6$ is thus calculated from linear regression of the 300 K lanthanide elpasolite series dataset to be 126.7 cm^{-1} at 20 K. On the other hand, the $4f^{12}$ crystal-field energy levels exhibit smaller temperature shifts, and $E(a\Gamma_5) = 124\ \mathrm{cm}^{-1}$ (deduced above from the hot electronic Raman transition). On cooling, the vibronic level $\Gamma_1 + \nu_5(\tau_{2g})$ therefore comes into resonance with the electronic level, $a\Gamma_5$. It is evident that the spectrum of Amberger, Rosenbauer, and Fischer[1] for $Cs_2NaTmCl_6$ at 29 K shows a weak feature at 127 cm^{-1}, in addition to bands at 108 and 147 cm^{-1}. This band is observed by us at 128 cm^{-1} at 120 K, but is not observed by us at the lower temperature of 20 K, and is assigned to the uncoupled τ_{2g} vibration (i.e., excited in the Γ_4 electronic state or some low-lying acoustic-phonon state). Note that at 120 K, features corresponding to the upper energy coupled state (144 cm^{-1}) and to the uncoupled phonon (128 cm^{-1}) are observed, but the band due to the lower-energy coupled state is not observed by us. The reason may be that the latter is mainly an *electronic* state so that the temperature 120 K is still not low enough to observe it resolved from the background [as in Fig. 3(d)]. As the temperature decreases the (uncoupled) phonon energy decreases also, to a value nearer to the electronic energy, and with more ions in the ground state so that more ions come into resonance.

The simplest model of the interaction between the $a\Gamma_5$ and $\Gamma_1 + \nu_5$ states utilizes first-order perturbation theory in a 2×2 representation in which the two basis functions are the first component of $|a\Gamma_5;0\rangle = |a\Gamma_5 1\rangle|0\rangle$ and $|\Gamma_1;\nu_5\rangle = |\Gamma_1\gamma_1\rangle|1\rangle$, respectively:

$$\begin{vmatrix} E(a\Gamma_5) - E & W \\ W & E(\Gamma_1 + \nu_5) - E \end{vmatrix} = 0, \tag{16}$$

where, from the low-temperature spectra, the two solutions of E—the coupled mode energies, are $E_1 = 108\ \mathrm{cm}^{-1}$ ($a\Gamma_5^c$) and $E_2 = 148\ \mathrm{cm}^{-1}$ ($a\Gamma_5^{c'}$). As mentioned above, the

unperturbed ν_5 phonon energy has the value 126.7 cm^{-1}. If the unperturbed energy $E(a\Gamma_5)=124$ cm^{-1} is taken [i.e, $\delta = E(\Gamma_1+\nu_5)-E(a\Gamma_5)=2.7$ cm^{-1}] then the matrix element, W, of the electron-phonon coupling Hamiltonian, $H_{e-p}\cong 20$ cm^{-1}. The intensity ratio of the 148 and 108 cm^{-1} bands at 20 K, for several excitation lines, is $2.22\pm 0.05{:}1$, with the higher-energy band being stronger.

We notice that both the electronic state $a\Gamma_5$ and the ν_5 phonon state are degenerate and there is a possibility of $T_2\times t_2$ type Jahn-Teller coupling. We hope to provide elsewhere a more accurate description of the interaction of the *degenerate* states than that given by Eq. (16). At any rate, the interaction mechanism proposed herein differs from that of Becker, in which the matrix element W of the interaction energy H_{e-p} is proportional to the thermal population of the electronic ground state.

The other electronic Raman transitions (at 370 cm^{-1} and 394 cm^{-1}) are not observed in the low-temperature spectrum of $Cs_2NaTmCl_6$ and this is consistent with the results from the theoretical calculation (Table I) where the coefficients of $|F_2|^2$ are smaller for these transitions than for the transition to $a\Gamma_5$. A band is also not observed at 56 cm^{-1} so that the magnitude of F_1 appears to be much smaller than that of F_2. However we do not provide values of the scattering parameters for $Cs_2NaTmCl_6$ in Table I because the effects of resonance scattering (120 K data) and electron-phonon coupling (20-K data) are not included in our theoretical JOA treatment. The coefficients of the squares of the scattering parameters in the table do however provide further evidence for the resonance enhancement of the transitions from $(^3H_6)\Gamma_4$ at 120 K. The inclusion of the 120 K Boltzmann factor for transitions from the initial level at 56 cm^{-1} shows that the intensities are calculated to be very weak under the conventional JOA theory.

J. Reassignment of the optical spectra of $Cs_2NaTmCl_6$

The above explanation for the striking changes observed in the Raman spectrum of $Cs_2NaTmCl_6$ as the temperature is decreased also serves to clarify the problems of assignment in the optical spectra of this compound. Further confirmation for the assignment of the two coupled electron-phonon states is obtained from the reanalysis of the $^3H_5\rightarrow{}^3H_6$ magnetic dipole (MD) emission transitions of $TmCl_6^{3-}$ (Ref. 22) because the agreement with calculated MD intensity ratios is satisfactory *only if* the redistribution of intensity from one $a\Gamma_5$ state to two coupled states ($a\Gamma_5^c$, $a\Gamma_5^{c'}$ inferred to be at 104 and 147 cm^{-1} respectively, from the *optical spectral* analysis of this transition) is taken into account. Furthermore, the intensity ratio of vibronic origins for transitions from $^1G_4, {}^3F_3, {}^3H_4, {}^3F_4$ to $(^3H_6)a\Gamma_5^c$ compared with those to $(^3H_6)a\Gamma_5^{c'}$ is measured to be constant. Taking the mean intensity ratio $1{:}1.5\pm 0.3$ for vibronic and MD transitions terminating upon $a\Gamma_5^c$ and $a\Gamma_5^{c'}$ respectively, (and assuming that the intensities for the corresponding transitions terminating on the phonon state $(\Gamma_1+\nu_5)$ are negligible), the composition of the wave functions $a\Gamma_5^c$ and $a\Gamma_5^{c'}$ is deduced from optical spectra to be

$$a\Gamma_5^c = 0.77a\Gamma_5 - 0.63(\Gamma_1+\nu_5),$$
$$a\Gamma_5^{c'} = 0.63a\Gamma_5 + 0.77(\Gamma_1+\nu_5). \quad (17)$$

This is in satisfactory agreement with the wave functions deduced from the values of W and δ from the Raman data. The $^3H_6$ energy-level fit is satisfactory when these revised energy-level assignments are utilized,[16] and some further reassignments in the electronic spectra of $TmCl_6^{3-}$ are discussed in Appendix B.

K. Electron-phonon coupled states of $Cs_2NaYbCl_6$

The Raman spectrum of $Cs_2NaYbCl_6$ is of interest because of the electron-phonon coupling between the potentially Jahn-Teller active first excited state, $(^2F_{7/2})\Gamma_8$, and the state $(^2F_{7/2})\Gamma_6+\nu_2(\epsilon_g)$, where one quantum of ν_2 is excited in the ground state. At room temperature one broad, weak band is observed at 211 ± 1 cm^{-1}, which is 17 cm^{-1} smaller than the magnitude of $\nu_2=228$ cm^{-1} calculated from linear regression of the plot of the energy of this mode at room temperature for Cs_2NaLCl_6 against atomic number. Amberger and co-workers[1,2,24] have described the behavior of this band when the temperature is decreased. We also find that at 20 K only one band is observed in this region, at 200 cm^{-1} [Fig. 4(g)]. Note that the energy of ν_2 would be expected to increase by ~ 10 cm^{-1} (i.e., $\nu_2\approx 240$ cm^{-1}) from 300 to 20 K for $Cs_2NaYbCl_6$, according to the trend for Cs_2NaLCl_6. Since the energy $E(\Gamma_8)$ of electronic state Γ_8 has not been determined exactly, the coupling element W is not estimated for this case.

It is noteworthy that only one lower energy (200 cm^{-1}) band is observed, not two as in the case of the coupled modes in $Cs_2NaTmCl_6$. Xia[5] has explained the absence of features from the low-temperature Raman spectrum of $TmPO_4$ as arising from radiationless decay of the electronic levels. For $Cs_2NaYbCl_6$, the upper coupled state of Γ_8 $\sim(\Gamma_6+\nu_2)$ coupling E_2 is likely to be ~ 250 cm^{-1} (by extrapolation of Fig. 5, refer to next section), so the state could decay by emission of two τ_{2g} phonons.

The JOA theoretical intensities of $\Gamma_6\rightarrow\Gamma_8$ and $\Gamma_6\rightarrow\Gamma_7$ (Table I) can be in agreement with experimental ones when $F_1=1.47$ and $F_2=1.82$ and the contribution of electron-phonon coupling is not included.

V. RAMAN SPECTRA OF MIXED CRYSTALS OF $Cs_2NaGd_{1-x}Yb_xCl_6$

The changes in the Raman spectrum that may result from doping a guest ion into a cubic lattice have been discussed by Manlief and Fan.[25] First, the $\mathbf{k}=0$ wave-vector selection rule is relaxed due to the loss of translational symmetry. Second, the loss of inversion symmetry at the L^{3+} site lowers the selection rules from O_h to subgroup O. Third, the substitution of guest ions may produce local modes and additional modes from defect pairs, triplets, etc.[26] For cubic $(NH_4)_2Te_xSn_{1-x}Cl_6$ a two-mode behavior has been observed,

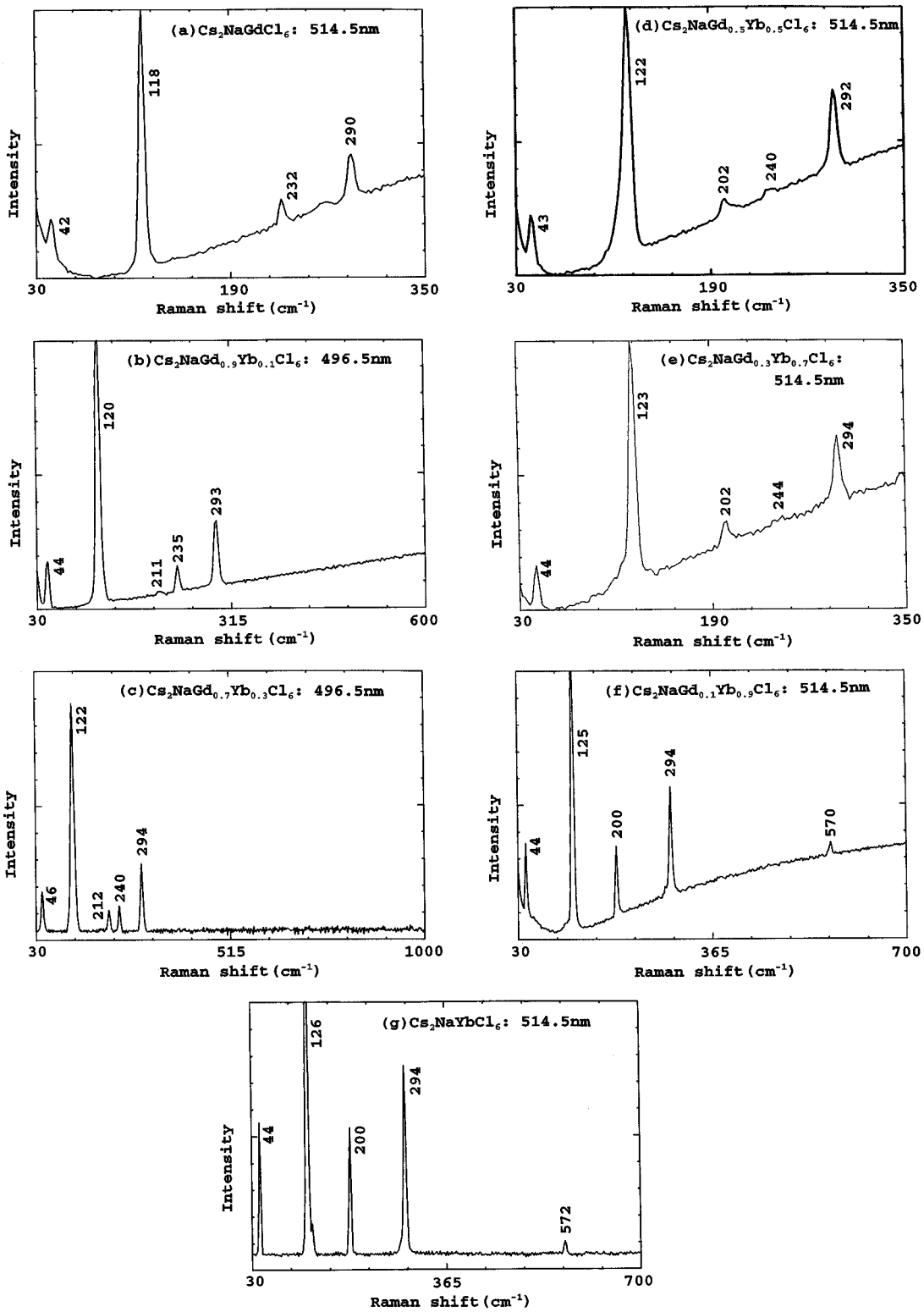

FIG. 4. 20-K Raman spectra of $Cs_2NaGd_{1-x}Yb_xCl_6$, $x=0$ to 1. The background has been subtracted in (c) and (g). The feature near 570 cm^{-1} in (f), (g) is too weak to be observed in the spectra of the dilute crystals and corresponds to the $(^2F_{7/2})\Gamma_6 \rightarrow \Gamma_7(^2F_{7/2})$ transition (Table I).

attributed to clustering in the mixed crystals.[27] Sliwczuk *et al.*[28] studied the Raman spectra of Cr^{3+} doped at low concentrations into hexafluoroelpasolite lattices and attributed many additional lines at low temperature to (i) the occurrence of phase transitions leading to reduction in symmetry and the change in soft-mode spectral activity; (ii) the local and resonant α_{1g} modes associated with Cr^{3+} sites.

In the present study the Raman spectra at 300 and 20 K have been investigated for $Cs_2NaGd_{1-x}Yb_xCl_6$, and the low-temperature results are shown in Fig. 4. At both tempera-

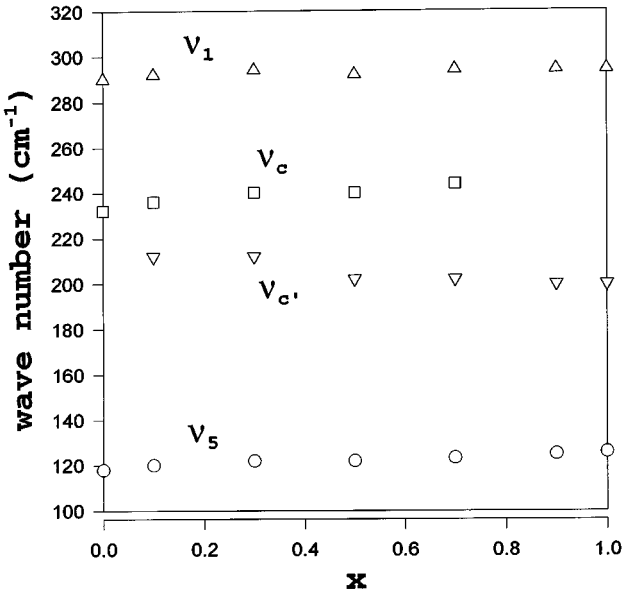

FIG. 5. Plot of the energies of the ν_1, ν_c, $\nu_{c'}$ and ν_5 modes at 20 K against the value of x in $Cs_2NaGd_{1-x}Yb_xCl_6$. ν_c and $\nu_{c'}$ refer to coupled electron-phonon modes, see text.

tures, the energies of the ν_1 and ν_5 modes increase linearly with parameter x. The intensity ratio ν_5/ν_1 shows a smooth decrease with increase in x, and the 300-K values are somewhat greater than those at 20 K. The behavior with change in concentration is unimodal and the energy shifts and relative intensity changes are similar to those for Cs_2NaLCl_6 in Fig. 1, so that the change in the vibrational force field acting upon $YbCl_6^{3-}$, and the site-symmetry perturbation are both of minor importance. The nearest-neighbor distance from one Yb to another is 0.755 nm.[29]

The behavior of the features related to $\nu_2(\epsilon_g)$ in the Raman spectrum of $Cs_2NaGd_{1-x}Yb_xCl_6$ between 200 and 250 cm^{-1} has been studied. In *neat* $Cs_2NaGdCl_6$ the ϵ_g mode is observed at 222 cm^{-1} at 300 K. The energy of this vibration is shifted 2 cm^{-1} higher in $Cs_2NaGd_{0.9}Yb_{0.1}Cl_6$. In the room-temperature spectrum of $Cs_2NaGd_{1-x}Yb_xCl_6$, $x=0.5,0.7$ both exhibit one broadband between 210 and 230 cm^{-1}, and the feature is still weak but more distinct at 209 and 212 ± 2 cm^{-1}, for $x=0.9$ and 1.0, respectively. The trend is clearer at 20 K (Figs. 4 and 5), where only one feature (232 or 200 cm^{-1}) is observed for $x=0$ or 0.9 and 1.0, but two bands are apparent for intermediate values. The results indicate that the higher-energy peak ($232-244$ cm^{-1}) is predominantly of $Cs_2NaGdCl_6$ character, whereas the lower energy peak ($200-212$ cm^{-1}) is predominantly of the lower-energy state resulting from the $\Gamma_8 \sim \Gamma_6+\nu_2$ coupling of $Cs_2NaYbCl_6$ discussed above. The relative intensities of these features are very sensitive to their energies, as shown in Figs. 4(b) and 4(c).

VI. CONCLUSIONS

The Raman spectra of Cs_2NaLCl_6 provide useful information concerning phonon levels and the location of the lower electronic multiplet crystal-field levels, which complements that available from optical spectroscopy. In the present study the relative intensities of the electronic Raman transitions have been calculated based on JOA theory, and the results are in reasonable agreement with experiment. The exceptions can be attributed to some cases in which the electron-phonon coupling has serious consequences, or resonance electronic Raman scattering occurs, or to cases where the terminal level undergoes fast nonradiative decay. In view of the limited experimental data, we have not provided best-fit calculated scattering intensity ratios but have provided representative values based on theory. As stated above, the JOA calculation does not give very good results for Ce^{3+} in $Cs_2NaCeCl_6$. In addition, if only the $4f^{n-1}5d^1$ configuration contributes, the ratio F_1/F_2 can be estimated to be 0.68. This ratio would provide a slightly worse fit to the Raman scattering than that given in Table I. In view of the relatively few crystal-field levels of the $4f^05d^1$ configuration, the JOA closure approximation by putting every intermediate configuration as degenerate, is likely to be most valid in this case. From the fitting values of the parameters for the lanthanide ions $L=$Pr,Eu in Cs_2NaLCl_6 (Table I) the mean ratio of F_1/F_2 is 0.22, close to the theoretical value of 0.25 quoted by Becker,[12] by assuming that the $4f^{n-1}5d^1$ configuration is the only intermediate configuration and $E(5d)=10^5$ cm^{-1}.

Excited-state electronic Raman transitions, initiating from the first excited level of $(^3H_6)\Gamma_4$ (at 56 cm^{-1}) in $Cs_2NaTmCl_6$, have been observed at 120 K. Under 476.5-nm resonant excitation into the $4f^n-4f^n$ vibronic structure of the $^1G_4$ multiplet the relative intensities of these transitions appear to increase slightly, compared with other excitation lines. A slight intensity enhancement of the electronic Raman bands was also observed in $Cs_2NaErCl_6$ under 496.5-nm excitation. The enhancement mechanism involves the mixing of opposite parity wave functions into the $4f^n$ electronic states by the vibronic operator, and not by the crystal field as in the lanthanide phosphates. The enhancement is not expected to be great because the oscillator strengths of individual vibronic transitions to the intermediate states are at most 10^{-7}. A more thorough study of the magnitude of the electronic Raman resonance enhancement is planned by using tunable dye-laser excitation.

Strong phonon-electron coupling is not unique to the system $YbPO_4$,[6] and it plays an important role in the Raman scattering of $Cs_2NaTmCl_6$ and $Cs_2NaYbCl_6$. A preliminary discussion has been given of the mechanism of this process. The present study has resolved the controversy concerning the assignment of the $^3H_6$ crystal-field levels of $TmCl_6^{3-}$.[22]

The Raman energies of the ν_1 and ν_5 moeity modes in $Cs_2NaGd_{1-x}Yb_xCl_6$ show a linear dependence upon concentration x, similar to the behavior in some other cubic mixed crystals.[30–32]

ACKNOWLEDGMENTS

P.A.T. thanks the HKUGC for partial financial support of this work under RG No. 904057 and 9040098, and the CLF for partial support of a visit by S.X.

APPENDIX A

Wave functions and energies of electronic states of L^{3+} in Cs_2NaLCl_6 from electronic absorption, emission, and excitation spectroscopy. The wave functions for $(^2F_{5/2},^2F_{7/2})Ce^{3+}$, $(^7F_{0,1,2})Eu^{3+}$, and $(^2F_{7/2},^2F_{5/2})Yb^{3+}$ were assumed to be pure.

L^{3+}	$^{2S+1}L_J$	Γ	Energy (cm^{-1})	Dominant terms in composition of wave function
Pr	$^3H_4$	Γ_1	0	$0.986(^3H_4)-0.163(^1G_4)+0.027(^3F_4)$
		Γ_4	235,249	$-0.977(^3H_4)+0.169(^1G_4)-0.098(a^3H_5)$
		Γ_3	417,428	$-0.977(^3H_4)+0.175(^1G_4)+0.076(^3H_5)$
		Γ_5	705	$0.983(^3H_4)-0.157(^1G_4)+0.066(^3F_3)$
		$a\Gamma_4$	2300	$0.926(a^3H_5)+0.358(b^3H_5)+0.113(^3H_4)$
		Γ_5	2400	$-0.989(^3H_5)+0.118(a^3H_6)-0.069(^3F_2)$
		Γ_3	2643	$-0.977(^3H_5)-0.158(^3F_2)+0.096(^3H_6)$
		Γ_3	4392	$0.990(^3H_6)+0.084(^3F_2)+0.083(^3H_5)$
		$a\Gamma_5$	4437	$0.826(a^3H_6)+0.538(b^3H_6)+0.117(^3F_2)$
		$b\Gamma_5$	4878	$0.793(b^3H_6)+0.461(a^3H_6)-0.345(^3F_2)$
		Γ_3	5203	$0.970(^3F_2)-0.162(^3H_5)+0.143(^1D_2)$
		Γ_5	5294	$0.910(^3F_2)-0.279(a^3H_6)+0.243(b^3H_6)$
		Γ_4	6613	$-0.976(^3F_3)-0.183(^3H_6)+0.068(b^3H_5)$
		Γ_5	6618	$-0.971(^3F_3)-0.133(b^3H_6)+0.113(^3F_4)$
Tm	$^3H_6$	Γ_1	0	$0.994(^3H_6)+0.093(^1I_6)+0.054(^3F_4)$
		Γ_4	56	$-0.995(^3H_6)-0.093(^1I_6)+0.037(^3F_4)$
		$a\Gamma_5$	123	$0.797(a^3H_6)-0.597(b^3H_6)+0.075(b^1I_6)$
		Γ_2	256	$0.995(^3H_6)+0.095(^1I_6)+0.007(^3F_3)$
		$b\Gamma_5$	370	$0.796(b^3H_6)+0.597(a^3H_6)+0.076(a^1I_6)$
		Γ_3	394	$0.995(^3H_6)+0.096(^1I_6)-0.014(^3F_4)$

APPENDIX B: ELECTRONIC ENERGY LEVELS OF $TmCl_6^{3-}$

The study of the emission spectra of $TmCl_6^{3-}$ in several elpasolite hosts, originating from five excited states and terminating on $^3H_6$, together with the assignment of hot bands in the absorption spectra, enabled the first three excited states to be assigned at 56 ± 1, 101 ± 4, and $145\pm1\ cm^{-1}$. The present study has shown that the latter two energy levels are derived from one parent electronic state, $a\Gamma_5$ with energy $124\ cm^{-1}$. The values are in agreement with those from the present study, in which the next highest level, Γ_2, has been assigned at $256\ cm^{-1}$. The $^3H_6$ energy-level fit is satisfactory when the revised energy-level scheme is employed.[16]

We have reanalyzed the vibronic structure of the 20-K emission spectra of $TmCl_6^{3-}$,[22] and observe that the transitions $^1G_4$, $^3F_3$, $^3H_4$, $^3F_4\rightarrow\Gamma_2+\nu_i(^3H_6)$, where $i=4$, are obscured by other transitions in all cases. However, two very weak bands which were previously given as tentative evidence for the observation of two-phonon modes are now seen to correspond to $^3H_4$, $^3F_3\rightarrow\Gamma_2+\nu_3(^3H_6)$, placing the Γ_2 level at $254\ cm^{-1}$. The assignment is confirmed by the observation of the 20-K emission band $(^3H_4)\Gamma_5\rightarrow\Gamma_2+\nu_6(^3H_6)$. [This feature was previously assigned to the lower energy ($243\ cm^{-1}$) component of a ν_3 vibronic origin, but it was then much stronger than the upper component. In the neat Cs_2NaLCl_6 elpasolites, the upper ($259\ cm^{-1}$) component is always stronger. The additional intensity of the $243\ cm^{-1}$ component thus arises from the coincidence with $(^3H_4)\Gamma_5\rightarrow\Gamma_2+\nu_6(^3H_6)$.] *The Γ_2 level is thus almost silent in the vibronic spectra.* Finally, it is apparent from the optical spectra that two coupled $a\Gamma_5$ levels are observed for $TmBr_6^{3-}$, with energies 74 and $108\ cm^{-1}$. Although the magnitudes of the crystal-field parameters are smaller for the hexabromoanion, the vibrational force constants are smaller too, so that the electron-phonon coupling also occurs between $a\Gamma_5$ and $\Gamma_1+\nu_5$.

[1] H.-D. Amberger, G. G. Rosenbauer, and R. D. Fischer, J. Phys. Chem. Solids **38**, 379 (1977).

[2] H.-D. Amberger, R. D. Fischer, and G. G. Rosenbauer, Transit. Met. Chem. **1**, 242 (1976).

[3] R. J. H. Clark and T. J. Dines, in *Advances in Infrared & Raman Spectroscopy*, edited by R. J. H. Clark and R. E. Hester (Heyden, London, 1982), Vol. 9. (A) Formulas (2) and (16); (B) Table II. (We have multiplied row 6 of the matrix in Table I, and column 6 of that in Table II each by -1.)

[4] R. J. Elliott, R. T. Harley, W. Hayes, and S. R. P. Smith, Proc. R. Soc. London Ser. A **328**, 217 (1972).

[5] S. Xia, Int. J. Mod. Phys. **6**, 59 (1991).

[6] P. C. Becker, G. M. Williams, N. M. Edelstein, J. A. Koningstein, L. A. Boatner, and M. M. Abraham, Phys. Rev. B **45**, 5027 (1992).

[7] S. Xia, in *Proceedings of Rare Earths Spectroscopy*, Changchun, China, edited by Su Qiang (World Scientific, Singapore, 1989), pp. 271, 275, 281.

[8] S. Xia, G. M. Williams, and N. M. Edelstein, Chem. Phys. **138**, 255 (1989).
[9] G. M. Williams, N. Edelstein, L. A. Boatner, and M. M. Abraham, Phys. Rev. B **40**, 4143 (1989).
[10] G. M. Williams, P. C. Becker, N. Edelstein, L. A. Boatner, and M. M. Abraham, Phys. Rev. B **40**, 1288 (1989).
[11] G. M. Williams, P. C. Becker, J. G. Conway, N. Edelstein, L. A. Boatner, and M. M. Abraham, Phys. Rev. B **40**, 4132 (1989).
[12] P. C. Becker, Ph.D. thesis, Lawrence Berkeley National Laboratory, University of California, 1986.
[13] L. R. Morss, M. Siegal, L. Stenger, and N. M. Edelstein, Inorg. Chem. **9**, 1771 (1970).
[14] J. D. Axe, Phys. Rev. A **136**, 42 (1964).
[15] J. C. Decius and R. M. Hexter, *Molecular Vibrations in Crystals* (McGraw-Hill, New York, 1977).
[16] P. A. Tanner, V. V. R. K. Kumar, C. K. Jayasankar, and M. F. Reid, J. Alloys Compounds **215**, 349 (1994).
[17] M. R. Roser, J. Xu, S. J. White, and L. R. Corruccini, Phys. Rev. B **45**, 12 337 (1992).
[18] H.-D. Amberger, G. G. Rosenbauer, and R. D. Fischer, Mol. Phys. **32**, 1291 (1976).
[19] R. W. Schwartz and P. N. Schatz, Phys. Rev. B **8**, 3229 (1973).
[20] P. A. Tanner and Y.-L. Liu, J. Alloys Compd. **204**, 93 (1994).
[21] P. A. Tanner, Mol. Phys. **63**, 365 (1988).
[22] P. A. Tanner, J. Chem. Phys. **85**, 2344 (1986), and references therein.
[23] P. A. Tanner, T. K. Choi, and K. Hoffman, Appl. Spectrosc. **47**, 1084 (1993).
[24] B. Kanellakopulos, H.-D. Amberger, G. G. Rosenbauer, and R. D. Fischer, J. Inorg. Nucl. Chem. **39**, 607 (1977).
[25] S. K. Manlief and H. Y. Fan, Phys. Rev. B **5**, 4046 (1972).
[26] D. W. Taylor, Phys. Rev. **156**, 1017 (1967).
[27] J. M. Zhang, S. C. Chen, T. Zhou, Y. B. Xie, Y. C. Xu, and J. Pelzl, Vib. Spectrosc. **3**, 299 (1992).
[28] U. Sliwczuk, R. H. Bartram, D. R. Gabbe, and B. C. McCollum, J. Phys. Chem. Solids **52**, 357 (1991).
[29] G. Meyer, Prog. Solid State Chem. **14**, 141 (1982).
[30] R. K. Chang, B. Lacina, and P. S. Pershan, Phys. Rev. Lett. **17**, 755 (1966).
[31] W. B. Lacina and P. S. Pershan, Phys. Rev. B **1**, 1765 (1970).
[32] C. Dujardin, B. Moine, and C. Pedrini, J. Lumin. **54**, 259 (1993).